Coordination and Organometallic Chemistry of Relevance to the Rhodium-Based Catalyst for Ethylene Hydroamination

Aurélien Béthegnies,[†] Vladislava A. Kirkina,[‡] Oleg A. Filippov,[‡] Jean-Claude Daran,[†] Natalia V. Belkova,[‡] Elena Shubina,[‡] and Rinaldo Poli[c]*,[†]

[†]CNRS, LCC (Laboratoire de Chimie de Coordination), Université de Toulouse, UPS, INP; F-31077 Toulouse, France; 205, route de Narbonne, F-31077 Toulouse, France

[‡]A. N. Nesmeyanov Institute of Organoelement Compounds, Russian Academy of Sciences, Vavilov Street 28, 119991 Moscow, Russia

S *Supporting Information*

ABSTRACT: The RhCl$_3$·3H$_2$O/PPh$_3$/nBu$_4$PI catalytic system for the hydroamination of ethylene by aniline is shown to be thermally stable by a recycle experiment and by a kinetic profile study. The hypothesis of the reduction under catalytic conditions to a Rh^I species is supported by the observation of a high catalytic activity for complex [RhI(PPh$_3$)$_2$]$_2$. New solution equilibrium studies on [RhX(PPh$_3$)$_2$]$_2$ (X = Cl, I) in the presence of ligands of relevance to the catalytic reaction (PPh$_3$, C$_2$H$_4$, PhNH$_2$, X$^-$, and the model Et$_2$NH amine) are reported. Complex [RhCl(PPh$_3$)$_2$]$_2$ shows broadening of the ^{31}P NMR signal upon addition of PhNH$_2$, indicating rapid equilibrium with a less thermodynamically stable adduct. The reaction with Et$_2$NH gives extensive conversion into cis-RhCl(PPh$_3$)$_2$(NHEt$_2$), which is however in equilibrium with the starting material and free Et$_2$NH. Excess NHEt$_2$ yields a H-bonded adduct cis-RhCl(PPh$_3$)$_2$(Et$_2$NH)···NHEt$_2$, in equilibrium with the precursors, as shown by IR spectroscopy. The iodide analogue [RhI(PPh$_3$)$_2$]$_2$ shows less pronounced reactions (no change with PhNH$_2$, less extensive addition of Et$_2$NH with formation of cis-RhI(PPh$_3$)$_2$(NHEt$_2$), less extensive reaction of the latter with additional Et$_2$NH to yield cis-RhI(PPh$_3$)$_2$(Et$_2$NH)···NHEt$_2$. The two [RhX(PPh$_3$)$_2$]$_2$ compounds do not show any evidence for addition of the corresponding X$^-$ to yield a putative [RhX$_2$(PPh$_3$)$_2$]$^-$ adduct. The product of C$_2$H$_4$ addition to [RhI(PPh$_3$)$_2$]$_2$, $trans$-RhI(PPh$_3$)$_2$(C$_2$H$_4$), has been characterized in solution. Treatment of the RhCl$_3$·3H$_2$O/PPh$_3$/nBu$_4$PI/PhNH$_2$ mixture under catalytic conditions yields mostly [RhCl(PPh$_3$)$_2$]$_2$, and no significant halide exchange, demonstrating that the promoting effect of iodide must take place at the level of high energy catalytic intermediates. The equilibria have also been investigated at the computational level by DFT with treatment at the full QM level including solvation effects. The calculations confirm that the bridge splitting reaction is slightly less favorable for the iodido derivative. Overall, the study confirms the active role of rhodium(I) species in ethylene hydroamination catalyzed by RhCl$_3$·3H$_2$O/PPh$_3$/nBu$_4$PI and suggest that the catalyst resting state is [RhCl(PPh$_3$)$_2$]$_2$ or its C$_2$H$_4$ adduct, RhCl(PPh$_3$)$_2$(C$_2$H$_4$), under high ethylene pressure.
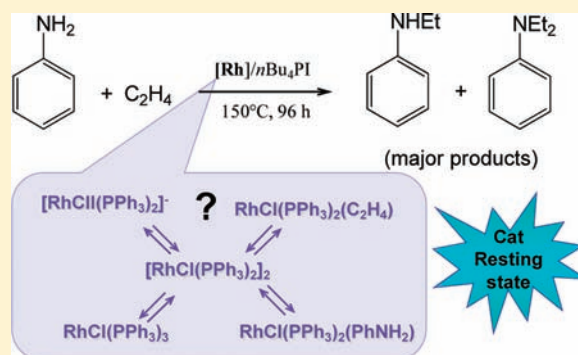
INTRODUCTION

An efficient halide-promoted platinum catalyst has recently been developed in our group for the hydroamination of ethylene and α-olefins by aniline derivatives.[1−6] This reaction yields N-ethylaniline (**1**) as major product, accompanied by traces of the double hydroamination product N,N-diethylaniline (**2**) and by minor amounts of quinaldine (**3**), see Scheme 1. Synthetic, spectroscopic and solution equilibrium studies[5,7,8] assisted by DFT calculations[9,10] have elucidated important mechanistic details of the hydroamination cycle and have rationalized experimental observations such as the halide promotion effects, the higher activity for the addition of less basic aniline derivatives, the strong preference for Markovnikov addition to higher olefins, and also hinted to the importance of the substrate and/or halide basicity in the deprotonation of a

Scheme 1. Products Observed in the Halide-Promoted Catalyzed Hydroamination of Ethylene by Aniline (MX$_n$/Y$^-$ = PtBr$_2$/Br$^-$ or RhCl$_3$·3H$_2$O/I$^-$)
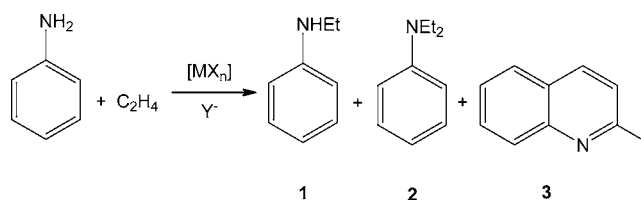
zwitterionic intermediate as a key step leading to catalyst deactivation.[11]

A few years ago, it has also been reported within our group that halides equally promote the aniline addition to ethylene when catalyzed by $RhCl_3·3H_2O/PPh_3$.[12] Compound $RhCl_3·3H_2O$ had previously been shown to efficiently catalyze the addition of basic secondary amines (Et_2NH, piperidine) to ethylene, albeit under rather forcing conditions, but the efficiency was greatly reduced for less basic amines or for higher olefins.[13,14] Subsequent work had shown that addition of PPh_3 to this system allows ethylene hydroamination by aniline, but only with much lower efficiencies.[15−17] A few well-defined complexes were also briefly investigated, giving low productivities and/or fast decomposition.[18−20] The work from our group has revealed that the same catalytic system, like $PtBr_2$, becomes much more active for the addition of aniline to ethylene when promoted by halide ions and the strongest promoting effect for this system turned out to be associated to iodide; under these conditions, greater amounts of double hydroamination product **2** were obtained relative to the $PtBr_2/Br^-$ system, whereas the quinaldine byproduct **3** was essentially absent.[12]

The promoting effect of halide ions in homogeneous catalysis is not unprecedented. For instance, the catalytic activity of a series of Ir(I) diphosphine complexes in intermolecular hydroamination (of norbornene by aniline), was shown to be greatly improved in the presence of fluoride ions,[21] whereas iodide is a recognized promoter for a variety of other catalyzed processes,[22] especially the Rh- and Ir-catalyzed methanol carbonylation. The origin of its promoting effect, however, is not always completely understood, being possibly associated to a number of possible causes, such as its good nucleophilicity, its redox activity, or simply its better binding to low-valent metal centers decreasing the tendency of the metal complex to precipitate and two or more effects may occur in different steps of the same catalytic cycle.[22] For the $PtBr_2$ hydroamination, as already stated, halides are also promoters and in that case bromide shows the strongest effect,[1] though only marginally better than iodide and the reasons of this difference are not yet understood.[11]

Given the rather reducing conditions imposed by the ethylene and aniline reagents (catalyst degradation to metallic rhodium was reported under certain conditions), it is reasonably assumed that $RhCl_3·3H_2O$ is transformed to a Rh^I complex, probably containing PPh_3 and iodide ligands, before beginning the catalytic cycle. However, the coordination chemistry of iodide complexes of Rh^I has been little explored, particularly with the set of ligands of relevance to this catalytic reaction. Complex $RhI(PPh_3)_3$ (the iodide equivalent of Wilkinson's catalyst) has been described by Wilkinson himself,[23] and the dinuclear complex $[RhI(PPh_3)_2]_2$ is also known.[23−25] With the notable exception of Vaska-type, CO containing complexes,[26,27] adducts with other ligands are scarce and this coordination chemistry merits renewed attention in view of this specific catalytic transformation.

Following the same strategy recently adopted for the study of the platinum-based catalyst,[5] we have decided to investigate well-defined rhodium complexes in terms of their solution equilibria in the presence of all available ligands under catalytic conditions (triphenylphosphine, ethylene, aniline, halide). DFT calculations have also been carried out to validate the experimental findings. Finally, additional catalytic tests have been run in the presence of well-defined Rh^I iodide complexes,

validating the concept that the active catalyst is indeed a Rh^I species.

■ EXPERIMENTAL SECTION

General. Unless otherwise stated, all manipulations were carried out under an argon atmosphere. Solvents were dehydrated by standard procedures and distilled under argon prior to use. Compounds $RhCl_3·3H_2O$ (Johnson Matthey 41.92%), PPh_3 (Aldrich 99%), nBu_4NCl (Fluka >97%) and nBu_4PBr (Acros Organics) were used as received. Tetra(n-butyl)phosphonium iodide was prepared from nBu_3P and $nBuI$ according to the literature[4] and stored protected from light and under argon in a freezer. Et_2NH (Fluka), $PhNH_2$ (Acros Organics; 99% for analysis ACS) and mesitylene (>97%, Fluka) were distilled and kept under argon in the dark. Ethylene (N25, purity ≥99.5%) was purchased from Air Liquide. Complexes $RhCl(PPh_3)_3$,[23] $[RhCl(PPh_3)_2]_2$,[23] $RhI(PPh_3)_3$,[24] and $[RhI(PPh_3)_2]_2$[24] were synthesized according to literature procedures. Single crystals of $RhI(PPh_3)_3$ were grown by diffusion of pentane into a dichloromethane solution.

Instrumentation. The GC analyses were performed on a Hewlett-Packard HP4890 (FID) chromatograph (HP 3395 integrator) equipped with a 30 m × 0.320 mm × 0.25 μm HP1 capillary column (DB-5MS). The NMR investigations were carried out on Bruker DPX 300 and AV300 spectrometers at 298 K operating at 300.13 MHz (^1H) and 121.495 MHz (^{31}P). IR measurements were carried out on Nicolet 6700 spectrometer using CaF_2 cell.

Reaction of RhCl(PPh₃)₃ with PhNH₂. In a 5 mm NMR tube was placed $[RhCl(PPh_3)_3]$ (10.7 mg, 0.012 mmol) and dissolved in ∼0.7 mL of CD_2Cl_2. The solution composition was checked by $^{31}P\{^1H\}$ NMR, revealing the presence of a minor amount of $[RhCl(PPh_3)_2]_2$ and free PPh_3, with which the starting compound is in equilibrium. $PhNH_2$ was added by microsyringe and the progress of the reaction monitored by $^{31}P\{^1H\}$ NMR. No change in the spectrum was observed upon introduction of up to 11 equiv of $PhNH_2$, except for the broadening of the doublet resonance of the dinuclear complex $[RhCl(PPh_3)_2]_2$.

Reaction of [RhCl(PPh₃)₂]₂ with Amines. *(a). PhNH₂.* In a 5 mm NMR tube was introduced $[RhCl(PPh_3)_2]_2$ (10.06 mg, 0.016 mmol) and dissolved in ∼0.7 mL of CD_2Cl_2. After checking the quality of the compound, $PhNH_2$ was added by microsyringe and the progress of the reaction monitored by $^{31}P\{^1H\}$ NMR, indicating only a weak affinity of this amine for bonding (see text).

(b). Et₂NH. In a 5 mm NMR tube was introduced $[RhCl(PPh_3)_2]_2$ (5.4 mg, 8.15 × 10^{-3} mmol) and dissolved in ∼0.7 mL of CD_2Cl_2. After checking the quality of the compound, Et_2NH was added by microsyringe and the progress of the reaction monitored by $^{31}P\{^1H\}$ NMR, giving evidence for quantitative formation of cis-$RhCl$-$(PPh_3)_2(Et_2NH)$ in the presence of excess Et_2NH (see text). A solution prepared separately in a Schlenk tube with the same concentration and excess Et_2NH was set out for crystallization by diffusion of a pentane layer, affording single crystals of $[RhCl$-$(PPh_3)_2]_2$.

Reaction of [RhI(PPh₃)₂]₂ with Amines. The reaction of compound $[RhI(PPh_3)_2]_2$ with both $PhNH_2$ and Et_2NH was carried out in CD_2Cl_2 inside an NMR tube, following the same experimental protocol described above for the related $[RhCl(PPh_3)_2]_2$ system.

Reaction of [RhI(PPh₃)₂]₂ with C₂H₄. Compound $[RhI(PPh_3)_2]_2$ (10 mg, 0.013 mmol) was suspended in 2 mL of CD_2Cl_2 in a Schlenk tube. The argon atmosphere was then replaced with ethylene and the suspension was stirred at room temperature. After a few minutes, the precipitate dissolved to yield a clear, yellow solution. ^1H NMR (CD_2Cl_2): δ 6.0−6.25 (30H, Ph), 4.43 (broad, 4H, C_2H_4). ^{31}P NMR (CD_2Cl_2): δ 35.8 (d, $^1J_{P-Rh}$ = 124 Hz). An analogous experiment was carried out in toluene-d_6, resulting in the same behavior except that the solubilization of the precursor required stirring for 24 h.

Ethylene Hydroamination Catalysis. *(a). Standard Catalytic Runs.* The catalytic experiments were conducted in a 100 mL stainless steel thermoregulated (electric oven) autoclave with a stirring bar. In a typical procedure, the autoclave was charged with $RhCl_3·3H_2O$ (34.2 mg, 0.13 mmol), $P(C_6H_5)_3$ (68.2 mg, 0.26 mmol) and nBu_4PI (3.26 g,

8.45 mmol), closed and submitted to several argon-vacuum cycles. Distilled and degassed aniline (4.1 mL, 45 mmol) was then syringed into the autoclave. The ethylene pipe was connected to the autoclave, purged, and the pressure was adjusted to 25 bar at RT. The temperature was then raised to 150 °C. After 96 h, the autoclave was allowed to cool down to room temperature and slowly vented. The reaction mixture was then poured into 120 mL of diethylether and the resulting suspension was stirred for 2 h and then filtered. The external standard N,N-di-n-butylaniline, (~0.15 g) was added to the collected ethereal phases and the solution analyzed by GC.

(b). Concentration Monitoring Experiments. An autoclave equipped with a siphon for sample withdrawal was charged with $RhCl_3 \cdot 3H_2O$, $P(C_6H_5)_3$, and nBu_4PI in similar amounts to the previous experiment, closed and submitted to several argon-vacuum cycles. Distilled and degassed aniline (4.1 mL, 45 mmol) and mesitylene (distilled and degassed, 16 mL) were then syringed into the autoclave. The dilution with mesitylene was necessary to allow the withdrawal of a sufficient number of samples. Ethylene was finally added and the reaction carried out as described above. Samples of ~0.5 mL were withdrawn are different times through the siphon and poured into 3.5 mL of diethylether, followed by stirring. The external standard N,N-di-n-butylaniline, (~0.010 g) was added to the collected ethereal phases and filtered before being analyzed by GC.

(c). Consecutive Catalytic Runs. A first catalytic run was carried out as described above in (a), until after venting the leftover ethylene from the autoclave. Degassed and distilled diethylether (50 mL) was syringed into the autoclave under an argon flow and the mixture was stirred for 2 h. After one hour of settling, the supernatant liquid was transferred from the autoclave to a collector flask through the siphon. The operation was repeated several times until the transferred liquid was colorless. The external standard N,N-di-n-butylaniline (~0.010 g) was added to the collected ethereal phases and filtered before being analyzed by GC. Subsequently, the autoclave was submitted to vacuum for 2 h and refilled with argon. A new charge of distilled and degassed aniline (4.1 mL, 45 mmol) was then syringed into the autoclave. Ethylene was then introduced and the second catalytic run as carried out as described in a, including the work up procedure.

Reaction of $RhCl_3 \cdot 3H_2O$ with PPh_3, Bu_4PI, and Aniline. In a Schlenk tube were introduced $RhCl_3 \cdot 3H_2O$ (34 mg, 0.13 mmol), PPh_3 (68.2 mg, 0.26 mmol), Bu_4PI (820 mg, 2.1 mmol). After purging with Ar, aniline (1 mL, 11.4 mmol) was added, and the resulting mixture was stirred at room temperature for 15 min, then at 150 °C for 16 h. The color of the mixture darkened to red-brown during the first 10 min of heating, then it did not further change. After cooling, 0.4 mL of the solution were transferred into a 5 mm NMR tube together with ~0.1 mL of CD_2Cl_2 for a ^{31}P NMR analysis (see text).

X-ray Crystallography. A single crystal of each compound was mounted under inert perfluoropolyether on the tip of a cryoloop and cooled in the cryostream of either an Agilent Technologies GEMINI EOS CCD diffractometer for $[RhCl(PPh_3)_2]_2$ or an Oxford-Diffraction XCALIBUR SAPPHIRE-I CCD diffractometer for $RhI(PPh_3)_3$. Data were collected using the monochromatic $MoK\alpha$ radiation ($\lambda = 0.71073$).

The structures were solved by direct methods (SIR97)[28] and refined by least-squares procedures on F^2 using SHELXL-97.[29] In compound $[RhCl(PPh_3)_2]_2$, some residual electron density was difficult to model. Therefore, the SQUEEZE function of PLATON[30] was used to eliminate the contribution of the electron density in the solvent region from the intensity data, and the solvent-free model was employed for the final refinement. There is one cavity of 238 Å per unit cell. PLATON estimated that the cavity contains 35 electrons which may correspond to a solvent molecule of dichloromethane as suggested by chemical analyses. All H atoms attached to carbon were introduced in idealized positions and treated as riding on their parent atoms in the calculations. The drawing of the molecules was realized with the help of ORTEP3.[31,32] Crystal data and refinement parameters are shown in Table 1.

Crystallographic data (excluding structure factors) have been deposited with the Cambridge Crystallographic Data Centre as supplementary publication no. CCDC 828152 and 828153. Copies

Table 1. Crystal Data and Structure Refinement

compound	$[RhCl(PPh_3)_2]_2$	$RhI(PPh_3)_3$
empirical formula	$C_{36}H_{30}ClP_2Rh$	$C_{54}H_{45}IP_3Rh$
formula weight	662.90	1016.62
temperature, K	180(2)	180(2)
wavelength, Å	0.71073	0.71073
crystal system	triclinic	orthorhombic
space group	$P\bar{1}$	$Pna2_1$
a, Å	9.7226(2)	19.7950(8)
b, Å	12.6361(3)	12.6130(6)
c, Å	13.7002(4)	17.7058(8)
α, deg	85.091(2)	90.0
β, deg	83.067(2)	90.0
γ, deg	79.384(2)	90.0
volume, Å^3	1638.78(7)	4420.7(3)
Z	2	4
density (calculated), Mg/m^3	1.343	1.180
abs coeff, mm^{-1}	0.723	1.211
$F(000)$	676	1556
crystal size, mm^3	$0.24 \times 0.19 \times 0.14$	$0.48 \times 0.37 \times 0.31$
θ range, deg	3.60 - 27.48.	2.99 - 26.37.
reflns collected	35493	24208
independent reflns (R_{int})	7439 (0.0337)	8931 (0.0234)
completeness, %	98.8	99.8
abs correction	multiscan	multiscan
max./min transmission	1.0/0.8750	0.7053/0.5941
refinement method	F^2	F^2
data/restraints/parameters	7439/0/361	8931/1/532
GOF on F^2	1.081	1.049
R1, wR2 $[I > 2\sigma(I)]$	0.0283, 0.0893	0.0236, 0.0558
R1, wR2 (all data)	0.0361, 0.0938	0.0275, 0.0570
absolute structure parameter		0.008(11)
residual density, e·Å^{-3}	0.487/−0.325	0.475/−0.753

of the data can be obtained free of charge on application to the Director, CCDC, 12 Union Road, Cambridge CB2 1EZ, U.K. (fax (+44) 1223-336-033; e-mail: deposit@ccdc.cam.ac.uk).

Computational Details. Calculations were performed with the Gaussian09 package[33] at the DFT/M06 level[34] without any ligand simplification. Effective core potentials (ECP) and its associated SDD basis set[35−38] supplemented with f-polarization functions (SDD(f))[39] were applied for rhodium atom and those supplemented with diffuse and polarization set of exponents (SDD(pd))[40] used for iodine atoms. Tests were also carried out using the 6-311G** basis set for the I atom,[41] leading to no difference for the relative energy of cis and trans isomers. The carbon and hydrogen atoms of the phenyl rings of PPh_3 ligands were described with 6-31G basis set; P atoms and organic ligands (C_2H_4, $PhNH_2$, Et_2NH) were described with a 6-31G(d,p) set of basis functions. Scaling factors were not applied to the calculated frequencies. Nonspecific solvent effects were introduced through SMD solvation model[42] by single-point energy calculations on gas phase optimized geometries for dichloromethane ($\varepsilon = 8.93$). The G^{SMD} values account for the solvation free energies, with inclusion of the solute free energy contributions $\Delta G^{SMD} = \Delta E^{SMD} + \Delta G^{gas} - \Delta E^{gas}$, where ΔE^{SMD} is the electronic energy plus the solvent entropy.[43]

■ RESULTS AND DISCUSSION

(a). Hydroamination Catalysis. Before addressing the chemistry of well-defined Rh^I complexes in solution, we present catalytic results that give additional information on the catalyst stability and mode of action. Within a previous $PtBr_2$-catalyzed investigation,[6] it has become obvious to us that the use of a glass liner, systematically used in previously published work, was causing an artificial decrease of the measured activity and a

Table 2. Hydroamination of Ethylene by Aniline Catalyzed by RhCl$_3$·3H$_2$O[a]

run	I⁻/Rh	I$_2$/Rh	conv./%	TON **1**	TON **2**	TON **3**	CE[b]
1	10		13(14)	42(47)	4(3)		49(53)
2	65		83(65)	50(130)	239(93)	1(4)	531(324)
3	150		69(65)	138(102)	100(120)	2(5)	341(352)
4	65	2	57(73)	150(28)	51(225)	(3)	251(484)
5	c		2	6	0	0	5
6(1)	65		73	28	229	1	488
6(2)			86	37	266	0	570

[a]Values in parentheses are those reported in the previous contribution.[12] Conditions: RhCl$_3$·3H$_2$O (34.2 mg, 0.13 mmol), PPh$_3$ (68.2 mg, 0.26 mmol, 2 equiv), n-Bu$_4$PI, PhNH$_2$ (4.1 mL, 45.5 mmol, 350 equiv), C$_2$H$_4$ (25 bar; ~770 equiv), 150 °C, 96 h. [b]CE (catalytic efficiency) = TON **1** + 2(TON **2**) + 2(TON **3**). [c]Same amounts of all reagents as in entry 2, in the absence of RhCl$_3$·3H$_2$O.

loss of reproducibility because of the high temperature conditions and the resulting condensation of aniline vapors in the catalyst-free zone of the autoclave underneath the liner. We have therefore repeated a selected number of previously reported experiments[12] without the glass liner in the autoclave. The results are shown in Table 2. Note that the catalytic reactions run with the RhCl$_3$·3H$_2$O/I⁻ catalyst require a much longer time (4 days) than those carried out with the PtBr$_2$/Br⁻ catalytic systems (10 h) in order to achieve reasonable conversions, because of the lower TOF of the former catalyst.

The catalytic efficiency (CE) is calculated on the basis of the number of cycles needed by the catalyst to yield each product (two cycles for **2** and **3**). As can be seen, while certain experiments gave essentially the same results (e.g., runs 1 and 3), others gave significantly improved conversions and catalytic efficiencies (run 2). All new results obtained without glass liner were repeated and found to be reproducible within 6%. The new results give the highest activity for a 65-fold excess of the iodide salt. Repetition of the experiment carried out in the presence of the I$_2$ additive, however, showed lower efficiency in the absence of the glass liner. The higher activity previously reported with glass liner has indeed been reproduced by us (an even greater catalytic efficiency of 542 has been obtained, which is essentially identical to the activity found without I$_2$ and without glass liner, entry 2). Hence, while I$_2$ was believed to have a promoting effect on the catalysis when this was carried out inside a glass liner, the opposite effect is found when the solution is in contact with the stainless steel autoclave walls. The reason for this change is currently not clear, but may be related to the negative interference, only after reaction with I$_2$, of unknown species chemisorbed on the autoclave walls. At any rate, the fact that the activity in the presence of I$_2$ when using a glass liner[12] is not better than that in the absence of I$_2$ without glass liner (run 2) shows that I$_2$ has no promoting effect on this catalysis. A control experiment run under the same conditions but without RhCl$_3$·3H$_2$O gave insignificant amounts of hydroamination (run 5).

One important question concerns catalyst deactivation, since this was shown to occur and to limit the TON for the related PtBr$_2$/Br⁻−catalyzed reaction: the catalyst turned into a black deposit (probably metallic Pt) with no residual catalytic activity.[6] To address this question for the Rh-based catalyst, we ran two subsequent experiments in the same autoclave under the same conditions as run 2, with the same catalyst charge, the second run being carried out after removing the product mixture of the first run, washing the solid catalyst several times (all operations were carried out inside the sealed autoclave under argon), and introducing a new charge of aniline and ethylene reagents (see details in the Experimental Section).

The results are shown in Table 2 (run 6). As clearly seen, a similar catalytic efficiency is obtained for the first and the second run, and both are in good agreement with those of the single run of entry 2. As a matter of fact, the discrepancy between the activities in the first and second run (the first being slightly smaller and the second slightly higher than for entry 2) is a bit greater than the usual reproducibility level mentioned above. We tentatively attribute this discrepancy to an incomplete recovery, in spite of several washings, of the products from the first run (there is a significant dead volume between the bottom of the autoclave and the siphon nozzle), which have therefore remained in the autoclave and added to those produced in the second run, artificially lowering the results of the first run and increasing those of the second one. At any rate, the experiment proves that the catalyst retains most of its activity after 4 days of operations at 150 °C. Hence, this catalyst is more robust than the PtBr$_2$/Br⁻ system.[1,6]

Additional information on the progress of the catalytic reaction was obtained by monitoring the substrate and product concentrations with time. The conditions used are those of entry 2 of Table 2, except that a diluent (mesitylene) was added to allow a sufficient number of sample withdrawals, again because of the large dead volume below the siphon nozzle. The results are shown in Figure 1a. The amount of aniline could not be determined accurately in this case because of peak overlap with the mesitylene diluent, but the peak separation was sufficient to demonstrate the essentially complete consumption of aniline at the end of the catalytic run. The conversion proceeded smoothly to first yield **1** and subsequently **2**, consistent with the notion that **1** is an intermediate in the generation of **2**. The absence of a notable induction time indicates a rapid conversion of the precatalyst to the active species. Quinaldine (**3**) was formed in small amounts throughout the reaction and it is not possible to conclude whether this reaction leading to this byproduct proceeds through **1** or not. The evolution of the sum of the three products (**1** + **2** + **3**) seems linear, suggesting zero-order in aniline. After 70 h, essentially no aniline is left in the mixture, and the sum of all products no longer increases, while the transformation of **1** into **2** continues to take place. The essentially complete aniline consumption is in line with the absence of catalyst deactivation, as already indicated above. The final mass balance is good, the three products accounting for >85% of the aniline amount charged in the autoclave, according to the GC calibration. A second reaction monitoring was also carried out with a double ethylene pressure (50 bar), giving very similar results, see Figure 1b.

In conclusion, these new catalytic experiments not only reproduce the basic findings reported in the previous
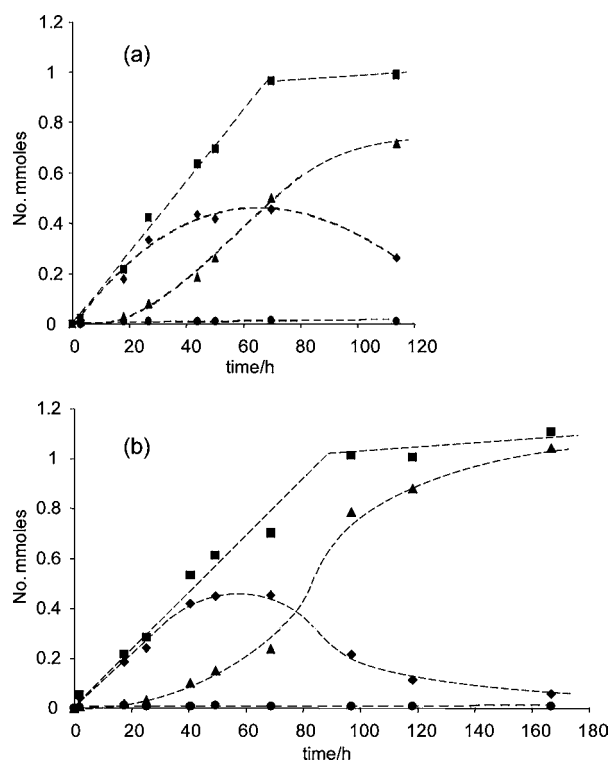
Figure 1. Kinetic profile of the $RhCl_3 \cdot 3H_2O$-catalyzed reaction between $PhNH_2$ and C_2H_4: 1 (◆), 2 (▲), 3 (●), 1 + 2 + 3 (■). (a) Conditions are the same as for entry 2 of Table 2. (b) Conditions are the same as for entry 2 of Table 2, except for a double C_2H_4 pressure (50 bar, ~1440 equiv).

contribution,[12] but also show that higher and more reproducible results are obtained in the absence of a glass liner (a negative effect of I_2 under this conditions remains to be rationalized) and demonstrate that the catalyst does not degrade under these conditions and furthermore give additional insights into the kinetic profile of the catalyzed transformation.

(b). Hydroamination with $[RhI(PPh_3)_2]_2$. As stated in the Introduction, the presence of a reducing environment (ethylene, aniline) and of the PPh_3 ligand presumably reduces the $RhCl_3 \cdot 3H_2O$ precatalyst to a Rh^I-PPh_3 complex. Furthermore, since the catalytic activity of $RhCl_3 \cdot 3H_2O$ is best promoted by the iodide ion, we initially assumed that the active species is a Rh^I-I complex. Indeed, iodide derivatives of Rh^I can been prepared by salt metathesis from the chlorido analogues and an iodide salt.[25] To test this hypothesis, we have carried out a catalytic run with the $[RhI(PPh_3)_2]_2$ complex as a precatalyst,

Table 3. Hydroamination of Ethylene by Aniline Catalyzed by $[RhI(PPh_3)_2]_2$[a]

run	I^-/Rh	conv./%	TON **1**	TON **2**	TON **3**	CE[b]
7	65	74	144	116	0	377
8	1	1	2	0	0	1

[a]Conditions: $[RhI(PPh_3)_2]_2$ (98.1 mg, 0.13 mmol of Rh), $PhNH_2$ (4.1 mL, 45.5 mmol, 350 equiv), C_2H_4 (25 bar; ~770 equiv), 150 °C, 96 h. [b]CE (catalytic efficiency) = TON **1** + 2(TON **2**) + 2(TON **3**).

both with and without the addition of excess free iodide in the form of the tetra-*n*-butylphosphonium salt. The results are shown in Table 3.

Comparison of the result of run 7 with that of run 2 (Table 2) indicates that $[RhI(PPh_3)_2]_2$ indeed leads to efficient catalysis, although the activity is slightly lower than that obtained from the same amount of $RhCl_3 \cdot 3H_2O$. This difference is probably related to parallel reactions that occur during the $RhCl_3 \cdot 3H_2O$ catalyst reduction and conversion to the iodide system, which involve the chloride ions, ethylene, aniline and perhaps also PPh_3, and produce other species that possibly further promote the catalysis. The water present in the $RhCl_3 \cdot 3H_2O$ compound may also act as a catalysis promoter. The results strongly support the proposal that the active form of the hydroamination catalyst is indeed, as initially suspected, a Rh^I species, because run 7 was carried out with a Rh^I precatalyst and without any I_2 additive. Note also that essentially no activity was obtained when the experiment was carried out in the absence of the iodide salt promoter (run 8). This results perfectly parallels that reported for the $RhCl_3 \cdot 3H_2O/I^-$ system.[12]

We now report the results of our investigations of the coordination chemistry and the relative thermodynamic stability of various Rh^I complexes, both in the chloride and iodide versions, to learn more about the equilibria that may take place for the catalytic species under the catalytic hydroamination conditions.

(c). Chloride System. As known in the literature, complex $RhCl(PPh_3)_3$ (Wilkinson's catalyst) equilibrates in solution with the dinuclear complex $[RhCl(PPh_3)_2]_2$ and free PPh_3 to a different extent depending on solvent and concentration.[23] Most of our NMR studies were carried out in CD_2Cl_2 at ~10^{-2} M concentration, where this dissociation was visible albeit not extensive. A representative ^{31}P spectrum is shown in the Supporting Information (Figure S1), indicating <10% dissociation. Hence, the equilibrium shown in eq 1 is shifted to the left under our conditions, even in the absence of excess PPh_3. The experiments that will be described further down, carried out starting from the pure dinuclear compound, were inspired by the observed changes to the small doublet $^{31}P\{^1H\}$ resonance of this compound (δ 51.50 J_{PRh} = 196 Hz) when carrying out reactions on $RhCl(PPh_3)_3$.

$$2RhCl(PPh_3)_3 \leftrightarrows [RhCl(PPh_3)_2]_2 + 2PPh_3 \qquad (1)$$

The reaction between complex $RhCl(PPh_3)_3$ and ethylene has already been studied, since it represents a key step of the olefin hydrogenation process catalyzed by Wilkinson's catalyst.[23] It affords compound *trans*-$RhCl(PPh_3)_2(C_2H_4)$, which could be isolated, but the latter tends to lose ethylene to generate $[RhCl(PPh_3)_2]_2$, with which it is in rapid equilibrium (the ^1H NMR shows only one resonance for free and coordinated C_2H_4, the position of which shifts as a function of the C_2H_4 excess). These results indicate a relatively comparable stability for the two sides of eq 2. We recall these literature results here because we will compare them later with other equilibria and with the results of computational investigations of relative thermodynamic stability.

$$[RhCl(PPh_3)_2]_2 + 2C_2H_4$$
$$\rightleftarrows 2trans\text{-}RhCl(PPh_3)_2(C_2H_4) \qquad (2)$$
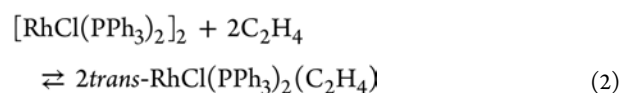
Exposure of $RhCl(PPh_3)_3$ to aniline, up to a large excess (>10 equiv) yielded no observable changes in the $^{31}P\{^1H\}$ NMR spectrum, except for a broadening of the doublet resonance of $[RhCl(PPh_3)_2]_2$. For this reason, the interaction of aniline was studied more in detail starting from the pure

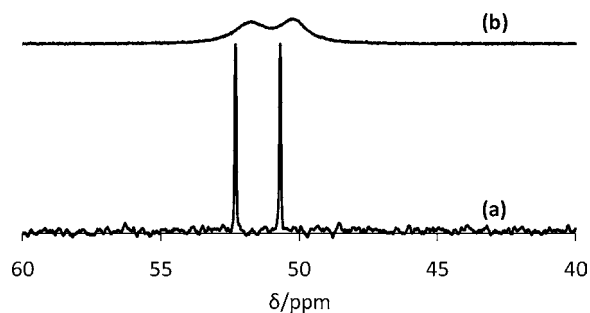dinuclear complex. The addition of a large excess of PhNH$_2$ (up to 65 equiv) did not reveal any new ^{31}P{^{1}H} resonance but

Figure 2. ^{31}P{^{1}H} study in CD$_2$Cl$_2$ of the interaction between [RhCl(PPh$_3$)$_2$]$_2$ (c = 0.027 M) and PhNH$_2$ in CD$_2$Cl$_2$. (a) Without PhNH$_2$. (b) With 65 equiv of PhNH$_2$. The difference in noise level is caused by a much larger number of accumulations for spectrum (b).

shows a significant broadening without major shifting of the resonance of compound [RhCl(PPh$_3$)$_2$]$_2$, as illustrated in Figure 2, suggesting a fast exchange between the reagents and the product (eq 3), strongly shifted to the reagents. Estimating a maximum amount of 1% product, given the conditions of temperature and concentrations, we can estimate that the product is at least 5.5 kcal mol^{-1} higher in free energy than the dinuclear precursor. On the other hand, the line broadening ($w_{1/2} \approx$ 150 Hz) gives us information on the pseudo-first-order exchange rate constant, yielding an estimated barrier of 14 kcal mol^{-1} for the aniline addition process.

$$[RhCl(PPh_3)_2]_2 + 2PhNH_2$$
$$\leftrightarrows 2RhCl(PPh_3)_2(PhNH_2) \qquad (3)$$
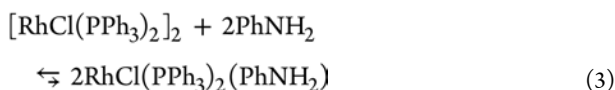
Given the difficulty in obtaining a stable amine derivative, we have oriented our investigation toward a more basic amine as a
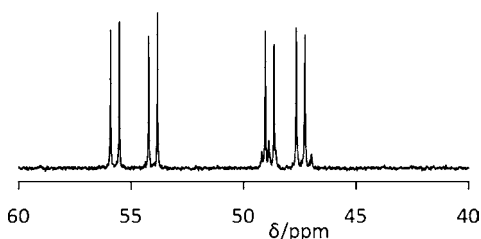

Figure 3. ^{31}P{^{1}H} NMR spectrum in CD$_2$Cl$_2$ of *cis*-RhCl-(PPh$_3$)$_2$(Et$_2$NH), obtained from [RhCl(PPh$_3$)$_2$]$_2$ and Et$_2$NH (5 equiv).

model system. The reaction of [RhCl(PPh$_3$)$_2$]$_2$ with Et$_2$NH gave rise to a new product, *cis*-RhCl(PPh$_3$)$_2$(Et$_2$NH). The ^{31}P{^{1}H} spectrum of the product of reaction 4 is shown in Figure 3. The two resonances in the form of doublets of doublets clearly indicate the cis stereochemistry, showing a mutual (PP) coupling of 47.5 Hz and couplings to the Rh nucleus by 207 Hz for the resonance at δ 55.0 and by 167 for that at δ 48.3. Note that no starting material remains visible in this spectrum (cf. Figure 2), and no other product peak is visible, notably there is no doublet that could indicate the formation of a trans isomer. The small signals flanking the doublet of doublets centered at δ 48.3 is the doublet of triplets of a small amount of RhCl(PPh$_3$)$_3$ contaminant (cf. Supporting

Information Figure S1; the corresponding doublet of doublets at δ 31.2, not shown in Figure 3, is also visible in the spectrum). Resonances of free PPh$_3$ and Ph$_3$PO are also observed in this spectrum. The ^{1}H spectrum shows, in addition to the large and unresolved multiplet resonance of the PPh$_3$ ligands in the aromatic region, broad resonances of the amine CH$_2$ and CH$_3$ protons at δ 3.15 and 1.60. In the presence of excess NHEt$_2$, these resonances remain distinguished from those of free NHEt$_2$, indicating slow exchange, but become sharper and notably the CH$_2$ resonance pattern is more complex than a binomial quartet, as expected since these protons become inequivalent (diastereotopic) upon coordination.

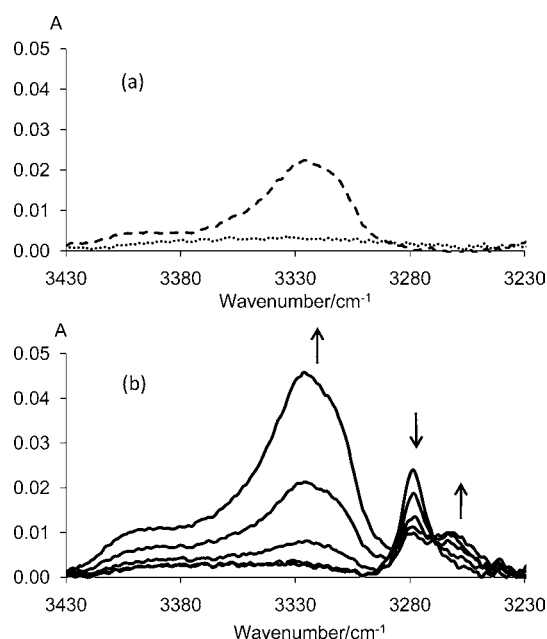A parallel IR study in the NH stretching vibration region showed the complete consumption of Et$_2$NH (ν_{NH} = 3327

Figure 4. Infrared study of the reaction of [RhCl(PPh$_3$)$_2$]$_2$ with NHEt$_2$ in CH$_2$Cl$_2$ (path length = 2.2 mm). (a) Spectra of [RhCl(PPh$_3$)$_2$]$_2$ (c = 6 × 10^{-3} M) (dotted line) and NHEt$_2$ (c = 0.05 M, dashed line). (b) Spectra of a 6 × 10^{-3} M solution of [RhCl(PPh$_3$)$_2$]$_2$ after addition of NHEt$_2$ with the successive concentrations (6, 12, 24, 60, and 120) × 10^{-3} M.

cm^{-1}, $\Delta\nu_{1/2}$ = 45 cm^{-1} ε = 2 L mol^{-1} cm^{-1}) at a 1:1 Et$_2$NH/Rh ratio and the appearance of a new narrower ν_{NH} band assigned to the coordinated amine (ν_{NH} = 3279 cm^{-1}, $\Delta\nu_{1/2}$ = 12 cm^{-1}), see Figure 4. This behavior is similar to that recently described for the PtBr$_2$(C$_2$H$_4$)(NHEt$_2$) complex.[8] Addition of Et$_2$NH beyond a Et$_2$NH/Rh ratio of 2 reduced the intensity of this new band in favor of yet another band at 3263 cm^{-1} ($\Delta\nu_{1/2}$ = 26 cm^{-1}), which can be attributed to the ν_{NH} vibrations of both coordinated and hydrogen bonded amine in a *cis*-RhCl-(PPh$_3$)$_2$(Et$_2$NH)·Et$_2$NH adduct on the basis of DFT calculations (vide infra). This evidence illustrates the presence of an H-bonding equilibrium, as detailed in eqs 4 and 5.

$$[RhCl(PPh_3)_2]_2 + 2Et_2NH$$
$$\rightarrow 2cis\text{-}RhCl(PPh_3)_2(Et_2NH) \qquad (4)$$

$$cis\text{-}RhCl(PPh_3)_2(Et_2NH) + Et_2NH$$

$$\rightleftarrows cis\text{-}RhCl(PPh_3)_2(Et_2NH) \cdot Et_2NH \qquad (5)$$
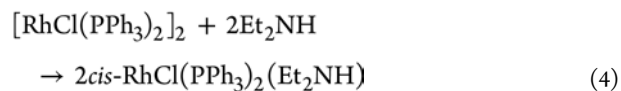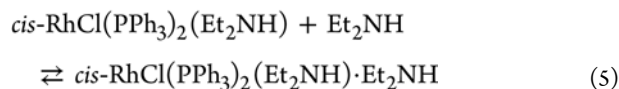
The literature is rather poor of reports of CO-free amine complexes of rhodium(I). A complex similar to cis-RhCl-$(PPh_3)_2(Et_2NH)$ was obtained by the same strategy (eq 4) with a substituted pyridine in place of Et_2NH, affording again a single product with cis geometry as confirmed by an X-ray structural analysis, but no ^{31}P NMR data were reported.[44] Complex $RhCl(PPh_3)_2(Et_2NSiMe_3)$, obtained by ligand exchange from $RhCl(PPh_3)_3$, on the other hand, shows only a single ^{31}P NMR resonance in agreement with a trans geometry.[45] It is possible in principle that the nonequivalence of the ^{31}P resonances for $RhCl(PPh_3)_2(Et_2NH)$ is caused by restricted rotation around the Rh–N in a trans structure, however in this case the $RhCl(PPh_3)_2(Et_2NSiMe_3)$ analogue would also be expected to have restricted rotation, since the amine is bulkier, leading to inequivalent P nuclei. We prefer to believe in an electronic effect of the amine ligand (the preference of a cis structure has also been confirmed by DFT calculations, vide infra). In further support of the assigned cis structure, the two $^{1}J_{PRh}$ and the $^{2}J_{PP}$ values observed for $RhCl(PPh_3)_2(Et_2NH)$ are very close to those reported for two different conformers of $RhCl(Ph_2PCH_2CH_2PPh_2)[N\text{-}(CH_2Ph)=C(Me)(C_6H_4\text{-}4\text{-}OMe)]$ where the cis conformation is enforced by the chelating nature of the diphosphine (203.5, 166.9, and 42.9 for one; 199.4, ~171, and 43.5 for the other), with the same pattern (higher $^{1}J_{PRh}$ for the lower field resonance).[46] We have attempted to crystallize the Et_2NH adduct and indeed single crystals were obtained from a solution that contained a large excess of $NHEt_2$ (5 equiv). However, the
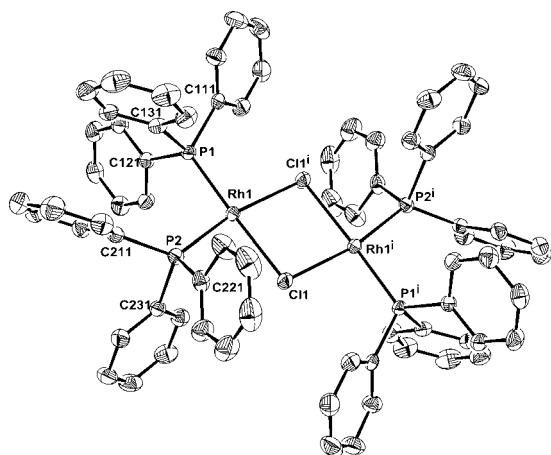
acetate per dimer,[47] whereas a crystal containing a disordered dichloromethane molecule was obtained under our conditions. A view of the molecule is reported in Figure 5. The structural details are in good agreement with those of the ethyl acetate solvate and no further comment on this structure is warranted.

In addition to PPh_3, C_2H_4, and $PhNH_2$, the hydroamination catalytic mixture also contains a halide salt. The study of the interaction between $RhCl(PPh_3)_3$ or $[RhCl(PPh_3)_2]_2$ and a halide salt was limited to chloride, introduced as the n-butylammonium salt, nBu_4NCl, to avoid the complication of mixed halide systems. The corresponding iodide system will be examined below. To put the maximum chances on our side, we studied the addition of Cl^- to the thermodynamically less stable dinuclear complex $[RhCl(PPh_3)_2]_2$, expecting to observe the product of equilibrium 6. However, the ^{31}P NMR spectrum of the solution, in the presence of as much as 10 equiv of nBu_4Cl, still showed the doublet resonance of the dinuclear starting material as the dominant resonance in the spectrum, unshifted and unbroadened relative to that of the pure starting material. Several other minor peaks, besides a peak of Ph_3PO, were also visible (spectrum shown in Supporting Information Figure S2), but it is impossible to assign any of them with certainty to the expected product of eq 6. The solution also shows instability, as additional small resonances became visible upon keeping the solution under argon for several hours. The resonance of $[RhCl(PPh_3)_2]_2$ always remained the dominant one, however. This experiment allow us to at least conclude that equilibrium 6, if any $[RhCl_2(PPh_3)_2]^-$ product is formed at all, must be heavily shifted to the left-hand side. Note that, on the other hand, the reaction of $[RhCl(CO)_2]_2$ with chloride generates $[RhCl_2(CO)_2]^-$ quantitatively.[48]

$$[RhCl(PPh_3)_2]_2 + 2Cl^- \rightleftharpoons 2[RhCl_2(PPh_3)_2]^- \qquad (6)$$
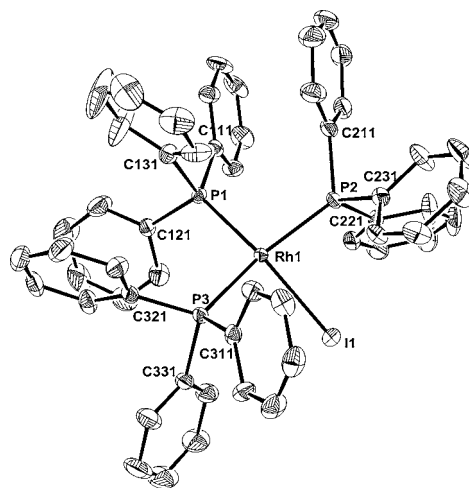

Figure 5. Molecular view of $[RhCl(PPh_3)_2]_2$ with the atom-labeling scheme. Displacement ellipsoids are drawn at the 50% probability level. H atoms have been omitted for clarity. Relevant bond distances (Å) and angles (deg): Rh–Cl, 2.4309(6); Rh–Cl^i, 2.3967(6); Rh–P1, 2.2021(6); Rh–P2, 2.2168(6). P1–Rh–P2, 96.05(2); P1–Rh–Cl1, 176.23(2); P1–Rh–Cl1^i, 95.24(2); P2–Rh–Cl1, 87.33(2); P2–Rh–Cl1^i, 168.01(2); Cl1–Rh–Cl1^i, 81.51(2); Rh–Cl1–Rh^i, 98.49(2). Symmetry transformations used to generate equivalent atoms: (i) $-x + 2$, $-y + 1$, $-z$.
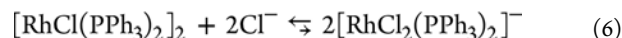

Figure 6. Molecular view of $RhI(PPh_3)_3$ with the atom-labeling scheme. Displacement ellipsoids are drawn at the 50% probability level. H atoms have been omitted for clarity. Relevant bond distances (Å) and angles (deg): Rh–I, 2.6840(3); Rh–P1, 2.2303(7); Rh–P2, 2.2937(7); Rh–P3, 2.3239(7). I–Rh–P1, 163.53(2); I–Rh–P2, 86.09(2); I–Rh–P3, 86.76(2); P1–Rh–P2, 97.38(3); P1–Rh–P3, 95.39(3); P2–Rh–P3, 157.89(3).

reversibility of eq 4 and the lower solubility of the dinuclear products led to the crystallization of the starting material. The molecular structure of $[RhCl(PPh_3)_2]_2$ has previously been reported in a habit containing an interstitial molecule of ethyl

(d). Iodide System. Although compound $RhI(PPh_3)_3$ is known,[23] its X-ray structure has apparently never been reported. The only reported structure with a Rh^IIP_3 coordination environment is apparently that of compound

RhI(diop)(PPh₃).[49] Compound RhI(PPh₃)₃ crystallizes with the full molecule in the asymmetric unit in the orthorhombic space group *Pna*2₁. A view of the molecule is shown in Figure 6. The presence of three sterically encumbering PPh₃ ligands forces the structure to deviate from the preferred square planar configuration toward a butterfly arrangement (trans angles around 160°). The same effect was previously noted for different polymorphs of the related RhCl(PPh₃)₃ compound.[50] The Rh−P distances in the iodide structure compare well with those in the two different chloride structures, with the two phosphine ligands trans to each other showing slightly longer distances relative to that trans to the halide. The latter has a marginally longer distance than the same ligand in the two chloride structures [2.225(4) and 2.214(4) Å]. The Rh−I distance is shorter relative to the above-mentioned diop complex [2.704(1) Å].[49]

As already described in the literature, complex RhI(PPh₃)₃ equilibrates in solution with the dinuclear species [RhI-(PPh₃)₂]₂ and free PPh₃, like the chloride analogue. The dinuclear species is favored to a greater extent for the iodide system and indeed the best preparation method of the dinuclear complex is by PPh₃ dissociation under thermal conditions in a solvent where the dinuclear product is less soluble and precipitates.[24] The literature also shows that PPh₃ dissociation is faster for RhI(PPh₃)₃ than for the corresponding chloride, since the ^{31}P resonances are broad at room temperature[25] and become sharper upon cooling. All these observations, reproduced in our hands, suggest that the Rh−PPh₃ interaction is weaker in the iodide system.

The reaction of [RhI(PPh₃)₂]₂ with C₂H₄ takes place readily in dichloromethane and more slowly in toluene, to afford *trans*-RhI(PPh₃)₂(C₂H₄) selectively (eq 7), as shown by the presence of only one doublet resonance in the ^{31}P NMR spectrum at δ 35.8 ($^1J_{P-Rh}$ = 124 Hz) in CD₂Cl₂. The possibility that a halogen exchange has occurred with the chlorinated solvent to yield *trans*-RhCl(PPh₃)₂(C₂H₄), besides being against the HSAB principle, is categorically excluded because the same experiment run in toluene-d_8 gave a doublet resonance at δ 36.4 ($^1J_{P-Rh}$ = 125 Hz), whereas the corresponding experiment using [RhCl(PPh₃)₂]₂ in place of [RhI(PPh₃)₂]₂ gave a doublet resonance at δ 34.9 (d, $^1J_{P-Rh}$ 129 Hz). The coupling constant in the CD₂Cl₂ spectrum matches well with that obtained for the iodide system but not with that obtained for the chloride system in toluene-d_8. The ^{1}H spectrum of *trans*-RhI-(PPh₃)₂(C₂H₄) shows a broad resonance for the ethylene ligand, like that reported in the literature[23] for the corresponding chlorido derivative. Note that this complex could not be isolated and an NMR spectrum was not reported in the original study by Wilkinson et al.,[23] where its generation was attempted from RhI(PPh₃)₃. Our results and those already available in the literature suggest that the ethylene binding constant to [RhI(PPh₃)₂] is smaller than for the chlorido analogue.

$$[RhI(PPh_3)_2]_2 + 2C_2H_4$$

$$\rightleftharpoons 2trans\text{-}RhI(PPh_3)_2(C_2H_4) \qquad (7)$$
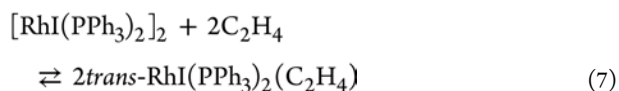
Addition of aniline, even in large excess, to [RhI(PPh₃)₂]₂ did not lead to any spectral change and notably, contrary to the chlorido system, did not significantly broaden the ^{31}P resonance, suggesting that the energy gap between the reactant mixture and the putative RhI(PPh₃)₂(PhNH₂) product is greater than for to corresponding chlorido system. Addition of

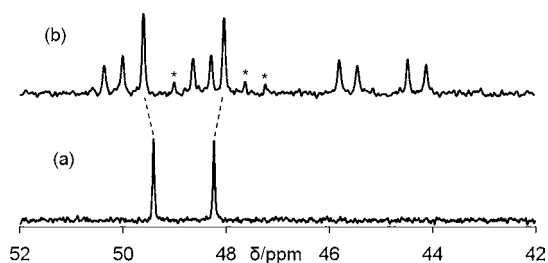**Figure 7.** ^{31}P{^{1}H} NMR spectra of [RhI(PPh₃)₂]₂ in CD₂Cl₂ before (a) and after (b) the addition of 3 equiv of Et₂NH. The starred peaks are due to a trace amount of chlorido derivative, RhCl(PPh₃)₂(NHEt₂) (cf. Figure 3).

Et₂NH, on the other hand, resulted in reaction and formation of the expected *cis*-RhI(PPh₃)₂(Et₂NH). The latter compound is characterized, like the above-described chlorido analogue, by two doublets of doublets for the two inequivalent PPh₃ ligands, see Figure 7. At variance with the chlorido system, the Et₂NH addition process was not quantitative, resonances of the starting dinuclear complex remaining visible even after adding an excess amount of amine. The J_{PRh} of the dinuclear compound in the two spectra of Figure 7 is the same (190 Hz; the spectra were taken at two different field strengths).

The IR study of the reaction showed the consumption of the free amine ν_{NH} band, accompanied by the appearance of the band of the coordinated amine at ν_{NH} = 3279 cm^{-1} ($\Delta\nu_{1/2}$ = 12 cm^{-1}). This frequency is identical to that of the chlorido
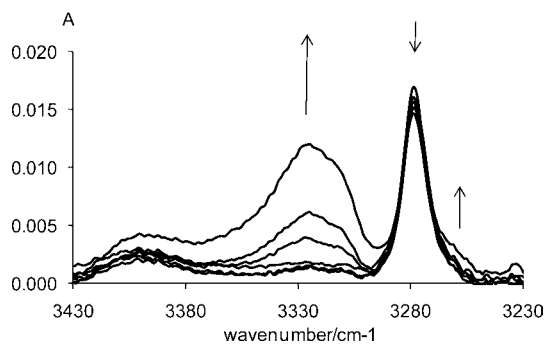

Figure 8. Infrared study of the reaction of [RhI(PPh₃)₂]₂ (c = 3 × 10^{-3} M) with NHEt₂ in CH₂Cl₂ (path length = 2.2 mm), after addition of NHEt₂ with the successive concentrations (3, 4.5, 6, 12, 18, and 30) × 10^{-3} M.

analogue, showing a negligible effect of the halide nature on the N−H stretching frequency. However, further addition of Et₂NH resulted in a much less significant change compared to the chlorido system. The lower frequency ν_{NH} band of the [RhI(Et₂NH)(PPh₃)₂]·Et₂NH adduct appeared in the spectrum only with a 10-fold excess of amine as a weak shoulder at ~3260 cm^{-1}, see Figure 8. This is in agreement with the computational results, showing less favorable formation of this adduct in case of iodide (vide infra).

Finally, addition of I$^-$ (in the form of its Bu₄N$^+$ salt, up to 3 equiv per Rh) to complex [RhI(PPh₃)₂]₂, like for the related experiment on the chloride system, resulted in no significant spectral change, indicating that equilibrium 8 is heavily shifted toward the left-hand side. Like for the chlorido analogue, the corresponding dicarbonyl complex [RhI₂(CO)₂]$^-$ is a well-known compound.[48]

$$[RhI(PPh_3)_2]_2 + 2I^- \rightleftharpoons 2[RhI_2(PPh_3)_2]^- \qquad (8)$$
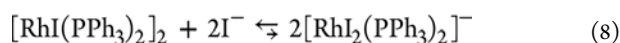
(e). Treatment of RhCl₃·3H₂O with PPh₃, Bu₄PI, and Aniline. A final spectroscopic investigation consisted of the ^{31}P NMR study of a mixture prepared with all the catalytic components (except for ethylene) under conditions mimicking those of the catalysis to gain further insights into the conversion of the RhCl₃·3H₂O precatalyst into the active catalyst. Excluding ethylene allows the reaction to be carried out in simple glassware (the boiling point of aniline is 184.13 °C). Thus, a mixture containing RhCl₃·3H₂O, PPh₃, *n*Bu₄PI, and PhNH₂ in a 1:2:16:88 ratio was kept at 150 °C for 16 h, even though no further change of color was noted after the first 10 min of heating. The *n*Bu₄PI/PhNH₂ ratio in this experiment
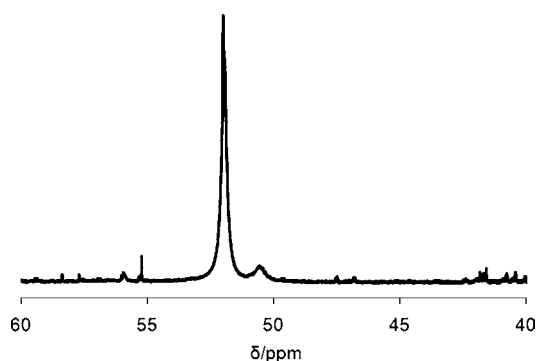

Figure 9. Excerpt of the ^{31}P{^{1}H} NMR spectrum of the final mixture generated from RhCl₃·3H₂O, PPh₃, *n*Bu₄PI, and PhNH₂ in a 1:2:16:88 ratio at 150 °C.

was identical to that of the catalytic runs, but the Rh and PPh₃ concentrations were ~4 times higher in order to facilitate the ^{31}P NMR measurement of the reaction products in the presence of the large excess of *n*Bu₄P$^+$ ion. The *n*Bu₄P$^+$ resonance was indeed by far the most intense one in the spectrum, but was accompanied by two major and relatively broad peaks, which account for most of the PPh₃ intensity, a stronger one at δ 52.0 and a smaller one at δ 50.6 (see Figure 9). The spectrum also showed a large number of other very weak resonances revealing the formation of many other products, none of which could be identified except Ph₃PO.

Comparison of chemical shift and line width indicates that the major product (δ 52.0) is $[RhCl(PPh_3)_2]_2$ (cf. Figure 2). The presence of the large excess of aniline is responsible for the resonance broadening as discussed above. The dinuclear iodide analogue, $[RhI(PPh_3)_2]_2$, does not appear to be present, since it should generate an unbroadened resonance centered at δ 48.8 (cf. Figure 7). It seems therefore reasonable to assume that the small resonance at δ 50.6 belongs to a mixed-halido species, Rh₂(I)(Cl)(PPh₃)₄, broadened by exchange with aniline like the chlorido dimer and unlike the iodido dimer.

The results of this experiment confirm therefore that RhCl₃·3H₂O is reduced to Rh^I under catalytic conditions in the presence of PPh₃, aniline, and iodide ions but reveal that no extensive halide exchange has taken place and the chlorido dinuclear species $[RhCl(PPh_3)_2]_2$ is the major reaction product, at least after cooling the mixture back to room temperature. The lack of extensive halide exchange may result from thermodynamic (the relative amount of iodide used here is 4 times less than in the catalytic run, but still in quite large excess relative to Rh) or kinetic factors. We believe that the reason is

thermodynamic. In support of this argument, we note that Cl/I halide exchange processes have been shown to favor the chlorido species also in other cases when carried out in the presence of soluble salts (e.g., CpMoI₂(PMe₃)₂ to CpMoICl-(PMe₃)₂ and CpMoCl₂(PMe₃)₂ with PPNCl/CH₂Cl₂;[51] MoOI₂(PMe₃)₃ to MoOICl(PMe₃)₃ and MoOCl₂(PMe₃)₃ with *n*Bu₄NCl/acetone[52]) whereas exchange in the opposite direction occurs in the presence of partially soluble alkali metal salts, presumably because of the lower solubility of the alkali metal chloride (e.g., CpMoCl₂(PMe₃)₂ to CpMoICl(PMe₃)₂ and CpMoI₂(PMe₃)₂ with NaI/THF;[53] MoOCl₂(PMe₃)₃ to MoOICl(PMe₃)₃ and MoOI₂(PMe₃)₃ with NaI/acetone;[52] and of stronger relevance to this work, RhCl(PPh₃)₃ to [RhI-(PPh₃)₂]₂ and free PPh₃ with LiI/toluene[25]). DFT calculations have also been conducted to address this point (vide infra). At any rate, whatever the reason for the lack of halide exchange, the absence of a notable induction time in catalysis suggests that $[RhCl(PPh_3)_2]_2$ is an active precatalyst, without the need to be converted to the iodide analogue. The results do not exclude that the real catalyst is one of the very minor and unidentified byproduct formed in the reaction. However, the catalytic activity demonstrated independently for $[RhI-(PPh_3)_2]_2$ lends credence to the hypothesis that the dinuclear Rh^I structure is indeed responsible for generating the active catalyst. If this is the case, then the promoting effect of iodide (much better than chloride)[12] must operate at the level of higher-energy catalytic steps, rather than at the level of the resting state.

The most important conclusions to be drawn from this experiment is that the resting state of the catalytic cycle must be either $[RhCl(PPh_3)_2]_2$ or *trans*-RhCl(PPh₃)₂(C₂H₄), because it is known from independent experiments reported here and in the literature that the reaction of $[RhCl(PPh_3)_2]_2$ (or the iodido analogue) with ethylene is equilibrated but more favorable than the additions of aniline or halide ions.

(f). DFT Calculations. No ligand simplification was made and the calculations were full QM, at the M06 level. The

Table 4. Comparison between DFT Optimized and Experimental Geometries (Distances in Å, Angles in Degrees)

	RhCl(PPh₃)₃		RhI(PPh₃)₃	
	DFT	exp^a	DFT	exp^b
Rh–X	2.440	2.404(4)	2.760	2.6840(3)
Rh–P(trans to X)	2.258	2.225(4)	2.278	2.2303(7)
Rh–P(trans to P)	2.340	2.304(4)	2.344	2.2937(7)
	2.361	2.338(4)	2.374	2.3239(7)
X–Rh–P(trans)	164.9	166.7(2)	161.5	163.53(2)
X–Rh–P(cis)	82.4	84.5(1)	85.3	86.09(2)
	85.1	85.3(1)	87.6	86.76(2)
P–Rh–P(trans)	156.5	159.1(2)	157.7	157.89(3)
P–Rh–P(cis)	101.6	97.7(1)	99.3	97.38(3)
	95.7	96.4(2)	94.1	95.39(3)

^{a}Data from ref 50. ^{b}This work.

geometries of the dinuclear $[RhX(PPh_3)_2]_2$ systems (X = Cl, I) and their ligand adducts $[RhX(PPh_3)_2(L)]$ with L = PPh₃, X$^-$, PhNH₂, Et₂NH and C₂H₄ have been optimized by DFT calculations. The optimized geometries are in good agreement with the available experimental structures, namely, those of RhCl(PPh₃)₃ (orange polymorph) available in ref 50 and RhI(PPh₃)₃ reported in the present work. A comparison is

available in Table 4. The largest deviation in the bond lengths is seen for the Rh−I bond (0.07 Å), the others being within 0.05 Å, whereas the angles are all calculated within 2° from the experimental values.

The calculated geometry of $[RhCl(PPh_3)_2]_2$ agrees with the experimental ones (both the previously reported ethyl acetate solvate[47] and the dichloromethane solvate reported herein) in terms of bond lengths and angles, except for the bending at the $Rh(\mu\text{-}Cl)_2Rh$ bridge, whereas the experimental structures have a flat core. As a matter of fact, the preference for a bent or flat geometry for edge-sharing square planar d^8–d^8 dimers rests on a delicate energetic balance, as previously discussed in detail.[54] Very similar structures of $[RhCl(PR_3)_2]_2$ complexes have been shown to adopt either a flat (e.g., $PiPr_3$,[55] in addition to the above-mentioned PPh_3 structures) or bent (e.g., PMe_3,[56] tBu_2PH,[57] $(C_2F_5)_2PCH_2CH_2P(C_2F_5)_2$,[58] and $iPr_2PCH_2CH_2PiPr_2$[59]) geometry, and the related $[RhF(PPh_3)_2]_2$ compound adopts either a flat[60] or bent[61] geometry

Table 5. Various Energetic Parameters (in kcal/mol) of $RhX(PPh_3)_2(L)$, Relative to Those of $1/2[RhX(PPh_3)_2]_2 + L$ (X = Cl, I; L = PPh_3, X^-, $PhNH_2$, Et_2NH, and C_2H_4)

compound	ΔE	ΔG^a	ΔE^{SMD}	$\Delta G^{SMD,b}$	$G_{solv}{}^c$
(a) chloride system					
$RhCl(PPh_3)_3$	−11.7	−3.8	−12.7	−4.7	−43.8
cis-$[RhCl_2(PPh_3)_2]^-$	−6.8	−9.1	8.2	5.8	−73.6
$trans$-$[RhCl_2(PPh_3)_2]^-$	−4.4	−10.8	13.4	7.1	−70.6
cis-$RhCl(PPh_3)_2(PhNH_2)$	−9.2	−3.7	−8.9	−3.4	−36.7
$trans$-$RhCl(PPh_3)_2(PhNH_2)$	3.2	6.4	1.1	4.3	−39.0
cis-$RhCl(PPh_3)_2(Et_2NH)$	−8.6	−3.1	−13.7	−8.2	−34.4
$trans$-$RhCl(PPh_3)_2(Et_2NH)$	5.2	9.2	−1.8	2.3	−36.2
cis-$RhCl(PPh_3)_2(C_2H_4)$	−4.7	−0.1	−8.8	−4.2	−33.8
$trans$-$RhCl(PPh_3)_2(C_2H_4)$	−6.2	−3.3	−10.4	−7.4	−33.8
(b) iodide system					
$RhI(PPh_3)_3$	−9.3	−0.8	−9.5	−1.0	−42.8
cis-$[RhI_2(PPh_3)_2]^-$	−0.9	−3.8	8.9	6.0	−69.1
$trans$-$[RhI_2(PPh_3)_2]^-$	−0.6	−5.5	11.5	6.5	−66.9
cis-$RhI(PPh_3)_2(PhNH_2)$	−6.4	−1.3	−5.3	−0.2	−35.6
$trans$-$RhI(PPh_3)_2(PhNH_2)$	3.3	6.4	2.1	5.3	−37.9
cis-$RhI(PPh_3)_2(Et_2NH)$	−5.8	0.5	−10.8	−4.6	−34.1
$trans$-$RhI(PPh_3)_2(Et_2NH)$	6.3	10.4	0.0	4.2	−35.4
cis-$RhI(PPh_3)_2(C_2H_4)$	−2.3	2.0	−5.4	−1.1	−32.6
$trans$-$RhI(PPh_3)_2(C_2H_4)$	−4.5	−2.5	−8.6	−6.6	−33.6

[a]Gas-phase at T = 298.15 K. [b]$\Delta E^{SMD} + (\Delta G - \Delta E)$ at 298.15 K. [c]Solvation free energy calculated by the SDM model for the given compound (values for the reagents: $[RhCl(PPh_3)_2]_2$, −56.5; $[RhI(PPh_3)_2]_2$, −56.1; PPh_3, −14.6; Cl^-, −60.3; I^-, −50.8; $PhNH_2$, −8.7; Et_2NH, −1.0, C_2H_4, −1.4).

in different crystal habits. The calculations suggest preference for a bent geometry for an isolated $[RhCl(PPh_3)_2]_2$ molecule, at least at this level of theory, thus the experimental observation of a flat structure is probably the consequence of crystal packing effects.

The relative energies (both electronic and Gibbs free energies) for all $RhX(PPh_3)_2(L)$ systems (L = PPh_3, X^-, $PhNH_2$, $NHEt_2$ and C_2H_4; X = Cl, I) are reported in Table 5.

They are calculated with respect to the precursor complex $[RhX(PPh_3)_2]_2$ and free ligands L according to eq 9. The direct comparison with the experimental data is complicated by several approximations, which are well-known in the area of computational chemistry applied to condensed phase thermo-dynamics, the most important one being probably the use of unquenched translational and rotational modes for the estimation of the condensed phase entropy. Ion pairing effects (neglected in our calculation) may also affect the results for the ionic species.

$$[RhX(PPh_3)_2]_2 + 2L \rightarrow 2RhX(PPh_3)_2(L) \qquad (9)$$
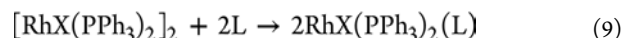
Solvent effects have also been included in the calculations using the SDM solvation model[42] in the CH_2Cl_2 medium (ε = 8.93) and this turns out to be important for the rationalization of certain trends. In particular, while solvation has either a negligible effect or favors the dimer splitting reaction by a few kcal/mol when adding a neutral ligand, it strongly disfavors the addition of X^-. This is attributable to the higher solvation energy of the free X^- ions relative to the neutral species (see Table 5, footnote c). Note that free X^- is not better solvated than the $[RhX_2(PPh_3)_2]^-$ ion, but the balance is shifted more in
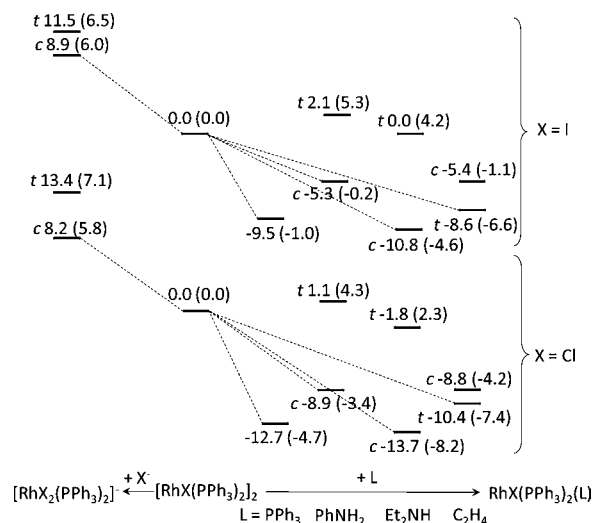

Figure 10. Relative ΔE^{SMD} and ΔG^{SMD} (in parentheses) in kcal/mol for geometry optimized $[RhX_2(PPh_3)_2]^-$ and $RhX(PPh_3)_2L$ (L = PPh_3, $PhNH_2$, Et_2NH and C_2H_4), relative to $[RhX(PPh_3)_2]_2$.

favor of the reactants side by the solvent, because the combination of $[RhX(PPh_3)_2]_2$ and $2X^-$ is better solvated than $2[RhX_2(PPh_3)_2]^-$. As expected, solvation free energy is higher for the systems containing the smaller Cl atom. The experimentally observed higher stability of the Et_2NH adduct relative to that of the $PhNH_2$ adduct is also reproduced by the calculation only when the solvent effect is included. The ΔE^{SMD} and ΔG^{SMD} parameters are graphically summarized in Figure 10.

Note that for all systems except the anionic ones, $\Delta G^{SMD} > \Delta E^{SMD}$ (the Gibbs parameter is more positive or less negative than the electronic energy), as expected from the reduction in molecularity (entropy decrease). The singular behavior for the anionic X^- adducts can be ascribed to the increase of rotational entropy for this system, because no rotational (or vibrational) modes are associated to the monatomic X^- reagent. Roughly speaking, since the major entropic contribution to the free

Table 6. Energies (in kcal/mol, Relative to RhX(PPh$_3$)$_2$(Et$_2$NH) (I) + 1/2 (Et$_2$NH···NHEt$_2$)) and Calculated N–H Stretching Vibrations (in cm^{-1})

compound	ΔE	ΔG^a	ΔE^{SMD}	$\Delta G^{SMD,b}$	$\nu(NH)^c$	$\nu(NH)^d$
(a) chloride system						
I + 1/2 (Et$_2$NH···NHEt$_2$)	0.0	0.0	0.0	0.0	3491	
II + 1/2 (Et$_2$NH···NHEt$_2$)	1.1	1.8	1.4	2.1	3392	
III	−2.2	7.4	−3.9	5.8	3496	3499
IV	−3.0	5.6	−2.4	6.3	3479	3448
V	−1.1	8.7	−0.5	9.3	3514	3434
VI	−1.3	8.9	−0.8	9.4	3430	3500
(b) iodide system						
I + NHEt$_2$	0.0	0.0	0.0	0.0	3503	
II + NHEt$_2$	1.4	1.0	2.4	2.0	3389	
III	−1.5	6.9	−3.9	4.5	3505	3488
IV	−1.8	4.7	−1.6	4.9	3473	3446
V	0.4	7.9	0.8	8.2	3508	3434
VI	0.3	8.1	−0.1	7.7	3442	3496

^{a}Gas-phase at T = 298.15 K. $^b\Delta E^{SMD}$ + (ΔG − ΔE) at 298.15 K. ^{c}Coordinated Et$_2$NH ligand. ^{d}H-bonded Et$_2$NH ligand.

energy change is given by changes in the translational and rotational modes, the reactions with the bidimensional (C$_2$H$_4$) or tridimensional (PPh$_3$, PhNH$_2$) ligands entail the disappearance of 3 translational and 3 rotational modes whereas the reaction with zero-dimensional X$^-$ entails on one hand the disappearance of 3 translational modes and on the other hand the generation of 3 rotational modes. This effect, predicted by the gas phase calculations, will obviously be attenuated in a condensed phase and further modulated by ion pairing.

The addition of L to [RhX(PPh$_3$)$_2$]$_2$ results in energetic stabilization except for the addition of X$^-$ (the solvent has an important effect on this equilibrium, as already pointed out above). Indeed, we were unable to observe any significant conversion of [RhX(PPh$_3$)$_2$]$_2$ in the presence of excess X$^-$. For the neutral ligands, the relative stability increases in the order PhNH$_2$ < C$_2$H$_4$ < PPh$_3$ < Et$_2$NH for each X on the ΔE^{SMD} scale. On the ΔG^{SMD} scale, on the other hand, the order is PhNH$_2$ < PPh$_3$ < Et$_2$NH < C$_2$H$_4$, in better agreement with the experimental evidence. Indeed, the RhCl(PPh$_3$)$_2$(C$_2$H$_4$) complex is sufficiently stable to be isolated, although it readily looses the ethylene ligand unless kept under a protecting ethylene atmosphere,[23] whereas we have shown above that the corresponding Et$_2$NH adduct also exists in solution but is not sufficiently stable to be isolated.

The energy change is less negative (or more positive) when X = I for all systems. In other words, [RhI(PPh$_3$)$_2$]$_2$ has a greater relative stability with respect to all its ligand adducts than the corresponding chloride system. This result is in agreement with all the available experimental evidence. Indeed, the more facile dissociation of PPh$_3$ from RhI(PPh$_3$)$_3$ or C$_2$H$_4$ from RhI(PPh$_3$)$_2$(C$_2$H$_4$) relative to the corresponding chloride systems has previously been discussed.[23] The new experiments reported in the present contribution also illustrate the lower stability of the other ligand adducts for the iodide system (vide supra).

Another notable result of the computational study concerns the relative stability for each pair of stereoisomers: the trans geometry is preferred for the C$_2$H$_4$ adduct, whereas all other ligand adducts show a preference for the cis geometry (moderate for X$^-$, strong for the amines). This is in perfect agreement with the experimental evidence, according to which the ethylene adduct is trans and the Et$_2$NH adduct reported in this contribution is cis, without the detection of the trans

isomer. The reason for the different stereochemical preference may be traced to the competition between the different π acceptors and π donors that are present in the coordination sphere. Thus, C$_2$H$_4$ is a stronger π acceptor and prefers to be located trans to a π donor halide ligand, leading to a preferred trans geometry, whereas the two more weakly π acceptor PPh$_3$ ligands avoid competing with each other in the cis geometry for the amine and X$^-$ adducts.

Given the infrared evidence for a secondary interaction between the RhX(PPh$_3$)$_2$(Et$_2$NH) complex and additional free Et$_2$NH, a calculation was also carried out for the RhX-(PPh$_3$)$_2$(Et$_2$NH)···NHEt$_2$ adducts. Four different minima could be located, the same ones for both halide systems. Adduct (**III**) derives from the lower energy RhX(PPh$_3$)$_2$(NHEt$_2$) molecule (**I**) and the other three (**IV**, **V** and **VI**) from a slightly higher energy minimum (**II**). Figure 11 shows a view of all the molecules for the Cl system (those of the I system are given in the Supporting Information). The relative energies and the calculated NH stretching frequencies are reported in Table 6. In order to take into account the H-bond breaking in the NHEt$_2$ reagent, the H-bonded dimer (Et$_2$NH···NHEt$_2$) has been chosen as a reference point.

Structures **I** and **II** differ in the orientation of the Et$_2$NH ligand relative to the rest of the molecule; the NH vector points toward one of the Ph rings of the cis-PPh$_3$ ligand in the lower energy **I** and toward the X ligand in the slightly less stable **II**. Structure **I** can only establish an H bond as a proton acceptor via the X ligand with the NH bond of the external NHEt$_2$ molecule, leading to **III**. Structures **IV** and **V** feature the same X···H–N interaction but also an additional N–H···N bond involving the coordinated amine as proton donor and the outer sphere amine as proton acceptor, whereas **VI** contains only the N–H···N interaction with the coordinated amine providing the proton to the external amine. The lowest energy structure is **III** when the solvation effects are taken into account, whereas **IV** is slightly favored in the gas phase. Note, however, that the energy difference between these two structures is small. The H-bonds are shorter in **IV**.

Structures **I** and **IV** also give the best agreement between the calculated ν_{NH} frequencies and the experimental data. Interestingly, the two NH vibrations in **IV** (for the coordinated and for the hydrogen bonded Et$_2$NH) appear at similar frequencies, slightly red-shifted from that of **I**. Considering the
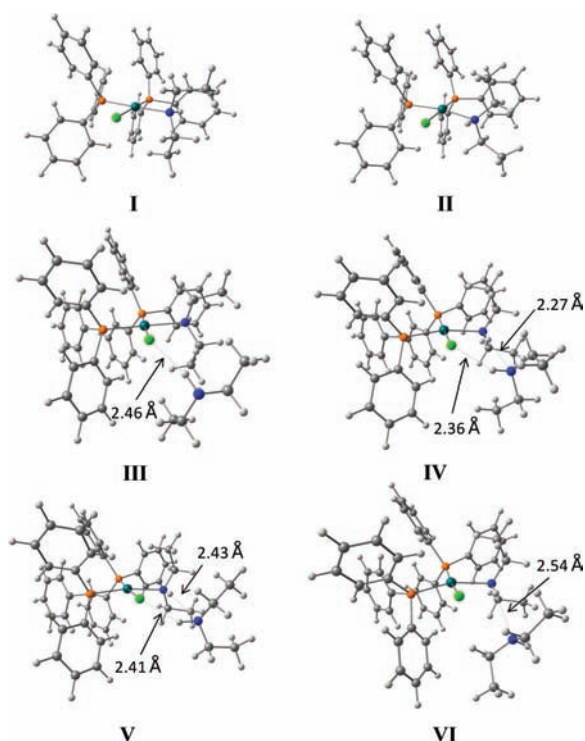
Figure 11. View of the optimized geometries of RhCl(PPh$_3$)$_2$(Et$_2$NH) (I and II) and RhCl(PPh$_3$)$_2$(Et$_2$NH)···NHEt$_2$ (III−VI).

expected difference between the frequencies computed in the gas phase and those experimentally measured in solution, these results allow the assignment of the experimentally observed band at 3263 cm^{-1} to a combination of the two ν_{NH} bands in **IV**. Finally, the data in Table 6 indicate a more favorable H-bond formation for the Cl system on the E scales (both gas phase and solution), whereas the process is more favorable for the I system on the Gibbs free energy scales. The experimental IR data are clearly demonstrating an easier formation of the H-bonded adduct for the Cl system, suggesting that the gas phase entropy correction is not adequate to address this phenomenon. Hence, the present system is yet another useful example pointing out to the care that one has to take when using computed gas phase thermodynamic data (even when including the solvation effects) for the prediction of solution behavior.

Table 7. Various Energetic Parameters (in kcal/mol) for Equilibrium (10), Depending on the Nature of the Countercation

cation	ΔE	ΔG^a	ΔE^{SMD}	ΔG^{SMD}
none	14.4	14.4	−4.1	−4.1[b]
Me$_4$N$^+$ [c]	−6.8	−5.8	−5.9	−4.8[b]
Me$_4$N$^+$ [d]			−5.2	−2.0
Me$_4$P$^+$ [d]			−4.9	−1.2
Na$^+$ [d]			−15.6	−14.9

[a]Gas-phase at T = 298.15 K. [b]ΔE^{SMD} + $(\Delta G - \Delta E)$ at 298.15 K. [c]Optimized in the gas phase and SMD calculation at the frozen geometry. [d]Optimization with SMD.

A final computational study has addressed the halide exchange equilibrium (10), of interest because of the somewhat unexpected lack of iodide incorporation into [RhCl(PPh$_3$)$_2$]$_2$

by treatment with excess nBu$_4$P$^+$I$^-$. The equilibrium has been analyzed in the presence of the free ions (no cation) as well as with ion pairs modeled by Me$_4$N$^+$X$^-$, Me$_4$P$^+$X$^-$, and Na$^+$X$^-$ and the relevant results are presented in Table 7. The results in the absence of cation are interesting since they show how much the right-hand side is favored by solvation with respect to the gas phase. Introduction of the Me$_4$N$^+$ cation indicates that the cation−anion association has a similar effect to that of the solvent model, since the gas phase parameters are essentially identical to those in solution. Optimization of the ion pair geometry in the presence of the solvent model does not greatly affect the results, relative to those obtained by correcting the gas phase energy by solvation effects, and the effect of Me$_4$N$^+$ and Me$_4$P$^+$ is essentially equivalent, whereas that of Na$^+$ differs significantly, stabilizing the right-hand side of the equilibrium by more than 10 kcal/mol. Clearly, the Na$^+$ results are not quantitatively relevant because NaCl and NaI are essentially insoluble in CH$_2$Cl$_2$. However, the stronger Na$^+$Cl$^-$ association relative to Na$^+$I$^-$, which is expected from first principles, is well reflected by the computed energy values, and the smaller solubility of NaCl than NaI (not known for CH$_2$Cl$_2$ solution, but confirmed in most polar aprotic organic solvents such as acetone and MeCN)[62] will in fact further accentuate the preference of equilibrium (10) for the right-hand side. Quantitative agreement with experiment is not achieved, since the equilibrium appears to be displaced to the left-hand side in the presence of soluble halide sources, however the calculated values are not too far from the expected outcome, considering that the calculation of free energy differences in condensed phases, especially when ionic species are involved, is one of the most challenging areas of computational chemistry, and the trend is as expected.

$$[RhCl(PPh_3)_2]_2 + 2I^-$$
$$\rightleftarrows [RhI(PPh_3)_2]_2 + 2Cl^- \qquad (10)$$
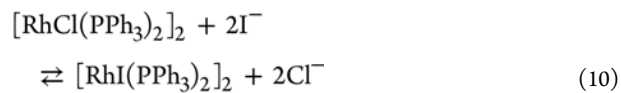
■ CONCLUSION

The present investigation has provided strong evidence that the recently reported[12] RhCl$_3$·3H$_2$O/I$^-$ catalyst for the hydroamination of ethylene by aniline is activated by reduction to a Rh^I active species. This catalyst is more robust than the PtBr$_2$/Br$^-$ system, no significant loss of activity after 4 days at 150 °C being observed in a recycle experiment, whereas the Pt-based catalyst is totally deactivated by the catalytic medium.[6,11] The catalytic activity of the Rh-based catalyst, however, is much lower than that of the Pt-based catalyst, as shown by the reaction kinetic profile. The solution studies of the [RhI-(PPh$_3$)$_2$]$_2$ system and of the chlorido analogue at room temperature show ligand addition equilibria to yield mononuclear RhX(PPh$_3$)$_2$(L) species (L = C$_2$H$_4$, PPh$_3$, PhNH$_2$, X$^-$, and the model Et$_2$NH amine) that are of comparable stability (marginally more stable according to DFT calculations, for C$_2$H$_4$, PPh$_3$, and Et$_2$NH; or less stable, for PhNH$_2$ and X$^-$). The reaction of RhCl$_3$·3H$_2$O in the presence of PPh$_3$, I$^-$, and PhNH$_2$ leads to [RhCl(PPh$_3$)$_2$]$_2$ as the major species, without notable halide exchange, thus suggesting that iodide is not needed at the level of the catalyst resting state. The effect of high temperature and pressure conditions on the equilibria cannot be easily predicted, but it may be speculated that either RhCl(PPh$_3$)$_2$(C$_2$H$_4$) or [RhCl(PPh$_3$)$_2$]$_2$ are the rate-determining intermediates (resting state) of the catalytic cycle. An ionic [RhClI(PPh$_3$)$_2$]$^-$ or [RhI$_2$(PPh$_3$)$_2$]$^-$ complex certainly does

12550

dx.doi.org/10.1021/ic201508m | Inorg. Chem. 2011, 50, 12539−12552

not appear to play a significant role, thus the promoting effect of iodide on the catalytic activity must be rationalized through its effect on the rate-determining transition state, which is still currently unknown. Future work will address the catalytic mechanism through computations.

■ ASSOCIATED CONTENT

Ⓢ Supporting Information

NMR spectrum of $[RhCl(PPh_3)_2]_2$, Cartesian coordinates of all optimized geometries (25 pages). This material is available free of charge via the Internet at http://pubs.acs.org. Crystallographic data (excluding structure factors) have been deposited with the Cambridge Crystallographic Data Centre as supplementary publication no. CCDC 833545. Copies of the data can be obtained free of charge on application to the Director, CCDC, 12 Union Road, Cambridge CB2 1EZ, UK (fax: (+44) 1223−336−033; e-mail: deposit@ccdc.cam.ac.uk).

■ AUTHOR INFORMATION

Corresponding Author
*Fax: (+) 33-561553003. E-mail: rinaldo.poli@lcc-toulouse.fr.

■ ACKNOWLEDGMENTS

■ REFERENCES

(1) Brunet, J. J.; Cadena, M.; Chu, N. C.; Diallo, O.; Jacob, K.; Mothes, E. *Organometallics* **2004**, *23*, 1264−1268.
(2) Brunet, J. J.; Chu, N. C.; Diallo, O. *Organometallics* **2005**, *24*, 3104−3110.
(3) Brunet, J.-J.; Chu, N.-C.; Rodriguez-Zubiri, M. *Eur. J. Inorg. Chem.* **2007**, 4711−4722.
(4) Rodriguez-Zubiri, M.; Anguille, S.; Brunet, J.-J. *J. Mol. Catal. A* **2007**, *271*, 145−150.
(5) Dub, P. A.; Rodriguez-Zubiri, M.; Daran, J.-C.; Brunet, J.-J.; Poli, R. *Organometallics* **2009**, *28*, 4764−4777.
(6) Dub, P. A.; Rodriguez-Zubiri, M.; Baudequin, C.; Poli, R. *Green Chem.* **2010**, 1392−1396.
(7) Dub, P. A.; Filippov, O. A.; Belkova, N. V.; Rodriguez-Zubiri, M.; Poli, R. *J. Phys. Chem. A* **2009**, *113*, 6348−6355.
(8) Dub, P. A.; Daran, J.-C.; Levina, V. A.; Belkova, N. V.; Shubina, E. S.; Poli, R. *J. Organomet. Chem.* **2011**, *696*, 1174−1183.
(9) Dub, P. A.; Poli, R. *J. Mol. Catal. A* **2010**, *324*, 89−96.
(10) Dub, P. A.; Poli, R. *J. Am. Chem. Soc.* **2010**, *132*, 13799−13812.
(11) Dub, P. A.; Béthegnies, A.; Poli, R., *Organometallics* accepted.
(12) Baudequin, C.; Brunet, J.-J.; Rodriguez-Zubiri, M. *Organometallics* **2007**, *26*, 5264−5266.
(13) Coulson, D. R. *Tetrahedron Lett.* **1971**, 429−430.
(14) Coulson, D. R. U.S. Patent 3,758,586 1973.
(15) Diamond, S. E.; Mares, F.; Szalkiewicz, A. *Fundam. Res. Homogeneous Catal.* **1979**, *3*, 345−358.
(16) Diamond, S. E.; Szalkiewicz, A.; Mares, F. *J. Am. Chem. Soc.* **1979**, *101*, 490−491.
(17) Diamond, S. E.; Mares, F. U.S. Patent 4,215,218, 1980.
(18) Steinborn, D.; Taube, R. *Z. Chem.* **1986**, *26*, 349−359.
(19) Krukowka, E.; Taube, R.; Steinborn, D. Patent DD 296,909 1991.
(20) Hahn, C.; Spiegler, M.; Herdtweck, E.; Taube, R. *Eur. J. Inorg. Chem.* **1999**, 435−440.
(21) Dorta, R.; Egli, P.; Zurcher, F.; Togni, A. *J. Am. Chem. Soc.* **1997**, *119*, 10857−10858.
(22) Maitlis, P. M.; Haynes, A.; James, B. R.; Catellani, M.; Chiusoli, G. P. *Dalton Trans.* **2004**, 3409−3419.
(23) Osborn, J. A.; Jardine, F. H.; Young, J. F.; Wilkinson, G. *J. Chem. Soc. A* **1966**, 1711−1732.
(24) Hartley, F. R.; Murray, S. G.; Potter, D. M. *J. Organomet. Chem.* **1983**, *254*, 119−26.
(25) Colebrooke, S. A.; Duckett, S. B.; Lohman, J. A. B.; Eisenberg, R. *Chem.—Eur. J.* **2004**, *10*, 2459−2474.
(26) Hughes, R. P. Rhodium. In *Comprehensive Organometallic Chemistry*; Wilkinson, G., Stone, F. G. A., Abel, E. W., Eds.; Pergamon: Oxford, U.K., 1982; Vol. 5, pp 277−540.
(27) Sharp, P. R. Rhodium. In *Comprehensive Organometallic Chemistry II*; Abel, E. W., Stone, F. G., Wilkinson, G., Eds.; Pergamon: Oxford, U.K., 1995; Vol. 8, pp 115−302.
(28) Altomare, A.; Burla, M.; Camalli, M.; Cascarano, G.; Giacovazzo, C.; Guagliardi, A.; Moliterni, A.; Polidori, G.; Spagna, R. *J. Appl. Crystallogr.* **1999**, *32*, 115−119.
(29) Sheldrick, G. M. *Acta Cryst. A* **2008**, *64*, 112−122.
(30) Spek, A. L. *J. Appl. Crystallogr.* **2003**, *36*, 7−13.
(31) Burnett, M. N.; Johnson, C. K. *ORTEPIII*, Report ORNL-6895; Oak Ridge National Laboratory: Oak Ridge, TN, U.S., 1996.
(32) Farrugia, L. J. *J. Appl. Crystallogr.* **1997**, *32*, 565.
(33) Frisch, M. J.; Trucks, G. W.; Schlegel, H. B.; Scuseria, G. E.; Robb, M. A.; Cheeseman, J. R.; Scalmani, G.; Barone, V.; Mennucci, B.; Petersson, G. A.; Nakatsuji, H.; Caricato, M.; Li, X.; Hratchian, H. P.; Izmaylov, A. F.; Bloino, J.; Zheng, G.; Sonnenberg, J. L.; Hada, M.; Ehara, M.; Toyota, K.; Fukuda, R.; Hasegawa, J.; Ishida, M.; Nakajima, T.; Honda, Y.; Kitao, O.; Nakai, H.; Vreven, T.; Montgomery, J., J. A.; Peralta, J. E.; Ogliaro, F.; Bearpark, M.; Heyd, J. J.; Brothers, E.; Kudin, K. N.; Staroverov, V. N.; Kobayashi, R.; Normand, J.; Raghavachari, K.; Rendell, A.; Burant, J. C.; Iyengar, S. S.; Tomasi, J.; Cossi, M.; Rega, N.; Millam, N. J.; Klene, M.; Knox, J. E.; Cross, J. B.; Bakken, V.; Adamo, C.; Jaramillo, J.; Gomperts, R.; Stratmann, R. E.; Yazyev, O.; Austin, A. J.; Cammi, R.; Pomelli, C.; Ochterski, J. W.; Martin, R. L.; Morokuma, K.; Zakrzewski, V. G.; Voth, G. A.; Salvador, P.; Dannenberg, J. J.; Dapprich, S.; Daniels, A. D.; Farkas, Ö.; Foresman, J. B.; Ortiz, J. V.; Cioslowski, J.; Fox, D. J. *Gaussian 09*, revision A.1; Gaussian, Inc.: Wallingford, CT, 2009.
(34) Zhao, Y.; Truhlar, D. G. *Theor. Chem. Acc.* **2008**, *120*, 215−241.
(35) Andrae, D.; Haussermann, U.; Dolg, M.; Stoll, H.; Preuss, H. *Theor. Chim. Acta* **1990**, *77*, 123−141.
(36) Haussermann, U.; Dolg, M.; Stoll, H.; Preuss, H.; Schwerdtfeger, P.; Pitzer, R. M. *Mol. Phys.* **1993**, *78*, 1211−1224.
(37) Kuchle, W.; Dolg, M.; Stoll, H.; Preuss, H. *J. Chem. Phys.* **1994**, *100*, 7535−7542.
(38) Leininger, T.; Nicklass, A.; Stoll, H.; Dolg, M.; Schwerdtfeger, P. *J. Chem. Phys.* **1996**, *105*, 1052−1059.
(39) Ehlers, A. W.; Bohme, M.; Dapprich, S.; Gobbi, A.; Hollwarth, A.; Jonas, V.; Kohler, K. F.; Stegmann, R.; Veldkamp, A.; Frenking, G. *Chem. Phys. Lett.* **1993**, *208*, 111−114.
(40) Check, C. E.; Faust, T. O.; Bailey, J. M.; Wright, B. J.; Gilbert, T. M.; Sunderlin, L. S. *J. Phys. Chem. A* **2001**, *105*, 8111−8116.
(41) Glukhovtsev, M. N.; Pross, A.; McGrath, M. P.; Radom, L. *J. Chem. Phys.* **1995**, *103*, 1878−1885.
(42) Marenich, A. V.; Cramer, C. J.; Truhlar, D. G. *J. Phys. Chem. B* **2009**, *113*, 6378−6396.
(43) Braga, A. A. C.; Ujaque, G.; Maseras, F. *Organometallics* **2006**, *25*, 3647−3658.
(44) Dowerah, D.; Radonovich, L. J.; Woolsey, N. F.; Heeg, M. J. *Organometallics* **1990**, *9*, 614−620.
(45) Petrucci, M. G. L.; Kakkar, A. K. *Organometallics* **1998**, *17*, 1798−1811.
(46) Ball, G. E.; Cullen, W. R.; Fryzuk, M. D.; Henderson, W. J.; James, B. R.; MacFarlane, K. S. *Inorg. Chem.* **1994**, *33*, 1464−8.

(47) Curtis, M. D.; Butler, W. M.; Greene, J. *Inorg. Chem.* **1978**, *17*, 2928−2931.

(48) Vallarino, L. M. *Inorg. Chem.* **1965**, *4*, 161−165.

(49) Brunner, H.; Zettler, C.; Zabel, M. *Z. Anorg. Allg. Chem.* **2003**, *629*, 1131−1135.

(50) Bennett, M. J.; Donaldson, P. B. *Inorg. Chem.* **1977**, *16*, 655−660.

(51) Poli, R.; Owens, B. E.; Linck, R. G. *Inorg. Chem.* **1992**, *31*, 662−667.

(52) Mata, J. A.; Maria, S.; Daran, J.-C.; Poli, R. *Eur. J. Inorg. Chem.* **2006**, 2624−2633.

(53) Linck, R. G.; Owens, B. E.; Poli, R.; Rheingold, A. L. *Gazz. Chim. Ital.* **1991**, *121*, 163−168.

(54) Aullon, G.; Ujaque, G.; Lledos, A.; Alvarez, S.; Alemany, P. *Inorg. Chem.* **1998**, *37*, 804−813.

(55) Binger, P.; Haas, J.; Glaser, G.; Goddard, R.; Kruger, C. *Chem. Ber.* **1994**, *127*, 1927−1929.

(56) Wang, K.; Goldman, M. E.; Emge, T. J.; Goldman, A. S. *J. Organomet. Chem.* **1996**, *518*, 55−68.

(57) Boettcher, H.-C.; Mayer, P. *Z. Naturforsch. B* **2008**, *63*, 1035−1039.

(58) Schnabel, R. C.; Roddick, D. M. *Inorg. Chem.* **1993**, *32*, 1513−1518.

(59) Oster, S. S.; Jones, W. D. *Polyhedron* **2004**, *23*, 2959−2965.

(60) Grushin, V. V.; Marshall, W. J. *J. Am. Chem. Soc.* **2004**, *126*, 3068−3069.

(61) Marshall, W. J.; Aullon, G.; Alvarez, S.; Dobbs, K. D.; Grushin, V. V. *Eur. J. Inorg. Chem.* **2006**, 3340−3345.

(62) Burgess, J. *Metal Ions in Solution*; Ellis Horwood: New York, 1978.